Rate of MgO Pickup in Alumina Inclusions in Aluminum-Killed Steel

DEEPOO KUMAR and PETRUS CHRISTIAAN PISTORIUS

This work aims to clarify the rate and mechanism of MgO pickup by alumina inclusions and the effect of oxide impurities in MgO crucibles on this transformation. Two MgO crucibles from different batches from the same supplier were used in laboratory experiments with Al-killed steel. A kinetic model was developed, based on mass-transfer control in the liquid steel. Rate constants were fitted using inclusion analysis. The rate of magnesium transfer from the two types of crucibles was found to differ by a factor of 20; faster magnesium transfer was associated with formation of a slag layer on the inner surface of the crucible wall (rather than a solid spinel product layer). The kinetic model was also used to simulate industrial scale ladle refining (1) to illustrate the effects of total oxygen concentration and (2) to evaluate the contribution of steel-refractory reaction (in addition to steel-slag reaction) on the rate of MgO pickup in alumina inclusion. The rate of MgO pickup was higher with a lower inclusion concentration. For ladle desulfurization, the extent of MgO pickup in inclusions is directly linked to the extent of desulfurization; both reactions are controlled by the oxygen potential at the steel-slag interface.

https://doi.org/10.1007/s11663-018-1436-z

I. INTRODUCTION

THIS work investigated the rate of transformation of alumina inclusions to magnesium spinel (xMgO Al_2O_3) by the transfer of dissolved Mg in steel from MgO refractory to inclusions.

In steel production, aluminum is commonly used to deoxidize steel during or after tapping steel from the steelmaking vessel (converter or electric arc furnace) into a ladle. Most of the alumina formed during deoxidation floats rapidly to the slag.[1] The remaining alumina inclusions can transform to spinel by Reaction [1]. In this reaction, brackets indicate elements dissolved in steel; the oxides can be pure species, dissolved in slag or in solid solutions. While Reaction [1] is written with stoichiometric MgO Al_2O_3 as the product, spinel is a solid solution extending from Mg/(Mg + Al) molar ratios of 0.20 to 0.63 at 1873 K.[2] The alternate version, Reaction [2], reflects the formation of MgO as the product; the MgO can form a spinel solid solution with Al_2O_3 or can be present as the periclase (MgO) phase.

$$3[Mg] + 4Al_2O_3 = 3MgO\,Al_2O_3 + 2[Al] \qquad [1]$$

$$3[Mg] + Al_2O_3 = 3MgO + 2[Al] \qquad [2]$$

Formation of spinel inclusions in liquid steels can be undesirable because spinel inclusions can cause nozzle clogging during continuous casting.[3]

In Al-killed steel, the source of [Mg] is reduction of MgO from slag or refractory, as shown by Reaction [3]; this reaction is simply the reverse of Reaction [2]. The local direction of the reaction is dictated by the local activities, with higher MgO activity or lower Al_2O_3 activity (or both) in the source of Mg (slag or refractory) than in the inclusions.

$$2[Al] + 3MgO = 3[Mg] + Al_2O_3 \qquad [3]$$

Both MgO-containing slag and MgO refractory can be the source of Mg in Reaction [3].[4–6] However, in some cases, MgO crucibles were found not to be efficient sources of [Mg][7,8] and a solid spinel layer at the steel-crucible interface appeared to retard Mg pickup by the steel.[8] The role of impurity oxides in increasing the rate of Mg pickup from an MgO crucible was studied in this work.

The other focus of this work was the rate of magnesium pickup by inclusions, in particular, the effect of the inclusion concentration on the measured pick-up rate. The expected reaction rate was calculated by assuming that mass transfer in steel to the steel-crucible interface was rate determining and also by using a

DEEPOO KUMAR and PETRUS CHRISTIAAN PISTORIUS are with the Center for Iron and Steelmaking Research, Carnegie Mellon University, Pittsburgh, PA 15213. Contact e-mail: pistorius@cmu.edu

Manuscript submitted July 31, 2018.
Article published online November 2, 2018.

FactSage macro method[9,10] to calculate the changing local equilibrium composition at the steel-crucible interface.

Several previous researchers[5,7,11] used magnesium pickup by inclusions to study the kinetics of transformation of alumina inclusions to spinel. A summary of the mass-transfer coefficients reported for previous laboratory-scale work is given in Table I. Liu *et al.*[5] considered magnesium transfer in liquid steel to be the rate-limiting step for the transformation of alumina inclusions to spinel inclusions (with Mg supplied by reaction between steel and MgO-C refractory). Okuyama *et al.*[7] concluded that magnesium transfer in the steel-slag boundary layer is the rate-limiting step and that diffusion within inclusions is fast (6-μm inclusions can completely transform to spinel within 20 seconds). Harada *et al.*[11] found that magnesium transfer is faster with steel-slag reaction than with steel-refractory reaction.

II. EXPERIMENTAL

In this work, steel was melted by radio-frequency induction heating of a graphite susceptor surrounding a slip-cast MgO crucible (61-mm internal diameter), as described in previous work.[12] In one experiment, a protective (argon) atmosphere was maintained by using a fused-quartz tube with gasket-sealed end caps as the furnace chamber[12]; in the other, an argon-flushed stainless-steel chamber was used. To produce the steel melt, 600 grams of electrolytic iron containing 7 ppm (by mass) of sulfur and approximately 350 ppm of oxygen was melted and then deoxidized by adding aluminum shot when the steel temperature was 1873 K $\pm$ 10 K. The aluminum was added through a port through the top of the furnace; steel samples were taken through the same port by immersing fused-quartz tubes (4-mm inner diameter) in the steel and using a pipette pump to draw steel into the tube.

The experimental conditions and sampling times are summarized in Table II. The experiments reported here were intended to be repeats. The MgO crucibles were from the same supplier but from different batches. The rate of magnesium pickup was found to be quite different; differences in crucible purity had a strong effect on the reactions. According to the crucible supplier, the maximum concentrations of impurities are 0.6 pct CaO, 0.2 pct SiO_2, 0.4 pct Al_2O_3, 0.1 pct Fe_2O_3, and 0.01 pct B_2O_3.

Figure 1(a) shows part of a cross section of the crucible wall before the experiment, and (b) shows the inner surface of the type 1 crucible after the experiment. The morphology of the inner surface of the used crucible indicated that a liquid layer had been present at the experimental temperature. No such layer had been present on the inner surface of the crucible wall before the experiment. In addition, no oxides (such as CaO and SiO_2) were added into the melt to facilitate the formation of a liquid phase on the crucible wall. The crucible contained $CaO\text{-}Y_2O_3$ particles (shown in the figure) as well as $CaO\text{-}Al_2O_3\text{-}SiO_2$ impurities. As shown in Figure 1(d), these impurities contributed to slag ($CaO\text{-}Al_2O_3\text{-}SiO_2\text{-}MgO\text{-}Y_2O_3$) formation on the inner surface of the crucible. From EDS analysis, the average Ca^{2+}/Al^{3+} ratio in the slag layer decreased from 1.5 to 0.5 during experiment 1. An increase in Al_2O_3 concentration in the slag layer is expected as a product of reduction of MgO from the slag layer by dissolved aluminum in liquid steel. Thus, the slag acted as an intermediary for Mg transfer to liquid steel from the MgO crucible: MgO from the crucible dissolved in the slag layer; Mg transfer to liquid steel occurred by reaction between the liquid steel and the slag layer. In contrast, the inner surface of the type 2 crucible was coated with a spinel layer after the experiment (Figure 1(c)). A similar product layer was found by Verma *et al.*,[8] who reported a low rate of formation of spinel inclusions in the liquid steel when a solid spinel layer formed on the crucible. A similar low rate of transformation of alumina to spinel was observed for the type 2 crucible in this work. The difference in the coating layer in these two experiments can be due to a difference in the chemical composition of the crucible (in particular, the concentration of impurities). It appears that, unlike the type 1 crucible, the type 2 crucible did not contain sufficient CaO-bearing impurities (such as $CaO\text{-}Y_2O_3$ or $CaO\text{-}Al_2O_3\text{-}SiO_2$) to form a liquid slag layer. In the absence of a slag layer, dissolved aluminum in the steel directly reacted with solid MgO at the steel-crucible interface, resulting in the formation of the solid spinel layer.

The steel samples taken during the experiments were mounted, ground, and polished to a 1 μm finish (using diamond suspension). Automated inclusion analysis was performed with an FEI/ASPEX Explorer scanning electron microscope (SEM) using optimized microscope settings, as described elsewhere,[13] yielding a spatial resolution of approximately 0.3 μm. In each case, an area of approximately 10 mm^2 was analyzed.

Table I. Summary of Mass-Transfer Coefficient in Steel Phase for Magnesium Transfer in Previous Laboratory Tests

Reference	k_{steel} (m/s)
Liu *et al.*[5]	5×10^{-4}
Harada *et al.*[11]	$0.7 - 1.5 \times 10^{-4}$
Okuyama *et al.*[7]	2×10^{-4}

Table II. Experiment Description

Experiment	Crucible	Addition	Sample Timing
1	MgO (type 1)	0.3 wt pct Al (t = 0)	3rd, 7th, 12th, 17th, 25th and 40th min
2	MgO (type 2)	0.16 wt pct Al (t = 0)	1st, 6th, 11th, 15th, 30th and 46th min

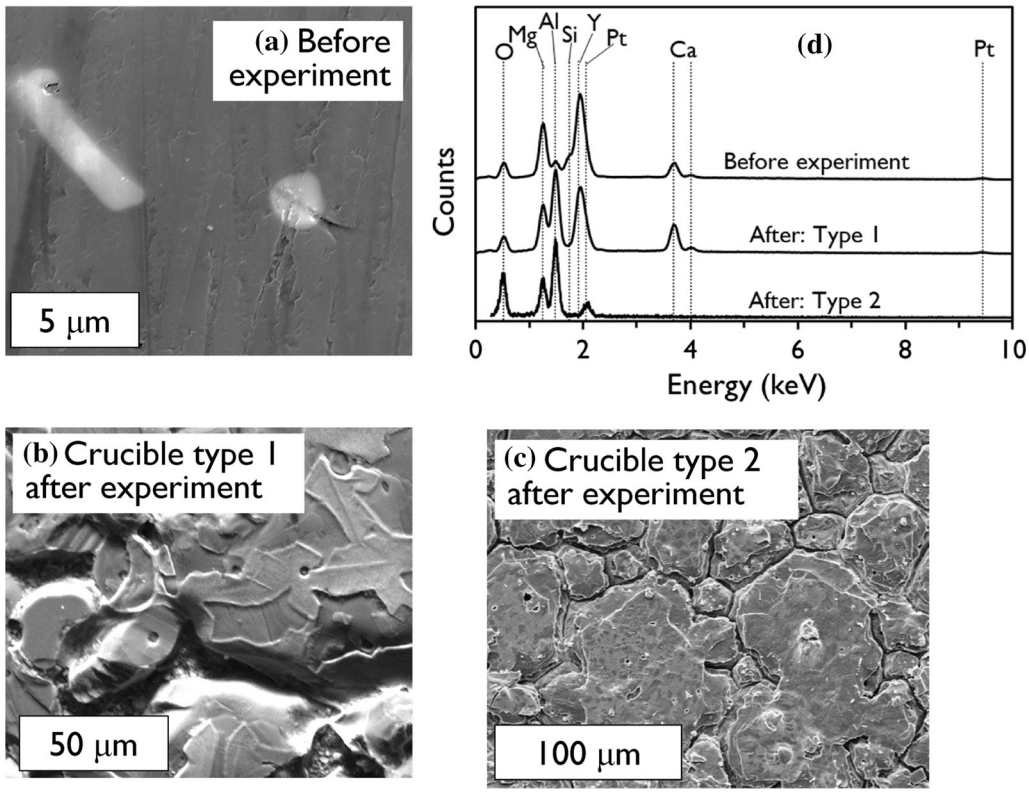

Fig. 1—Differences between type 1 and type 2 crucibles. (*a*) Cross section of the unused type 1 crucible (backscattered electron image), showing $CaO\text{-}Y_2O_3$ particles (bright) in the MgO matrix. (*b*) Inner surface of the type 1 crucible after the experiment, showing remains of a $CaO\text{-}Al_2O_3\text{-}MgO$ slag (secondary electron image). (*c*) The inner surface of the type 2 crucible was covered with spinel after the experiment (secondary electron image). (*d*) EDX spectra (10-kV accelerating voltage) confirming the compositions of the layers on the crucible wall; "before experiment" spectrum is of one of the bright particles in (a). The platinum peak was from the platinum coating sputtered onto the crucible sample for SEM analysis.

Microanalyses were performed at 10-kV accelerating voltage; counts of characteristic X-rays were converted to compositions in mass percentage by using the Merlet phi-rho-z algorithm.[14,15]

The area-based average composition of inclusions (expressed as the Mg:Al molar ratio) was calculated, as shown in Eq. [3], using each measured inclusion composition and its measured area on the polished surface.

$$(\text{Mg} : \text{Al})_{\text{average}} = \frac{\sum x_i A_i}{\sum A_i} \qquad [4]$$

where x_i is the Mg:Al molar ratio of each inclusion and A_i its cross-sectional area.

The mass fraction of inclusions was calculated from the measured inclusion area fraction (which is equal to the volume fraction):

$$\text{Mass fraction} = (\text{volume fraction}) \times \frac{\rho_i}{\rho_s} \qquad [5]$$

where ρ_i is the inclusion density (3990 kg/m^3 for Al_2O_3 and 3550 kg/m^3 for $MgAl_2O_4$[16]) and ρ_s is the density of steel (7800 kg/m^3).

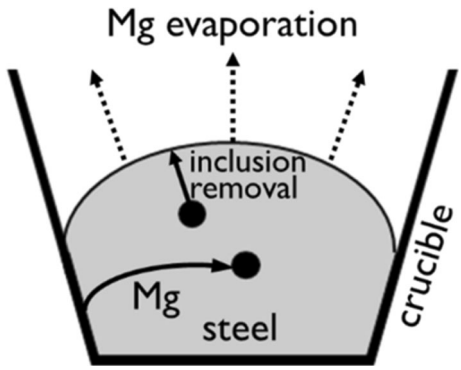

Fig. 2—Schematic of reactions involved in magnesium transfer during reactions involving steel, the crucible, inclusions, and the surrounding inert gas.

III. MODELING

Changes in inclusion composition and concentration were modeled by considering (1) inclusion removal from the melt, (2) the reaction between steel and the MgO crucible, (3) loss of magnesium from liquid steel by evaporation, and (4) the steel-inclusion reaction (Figure 2).

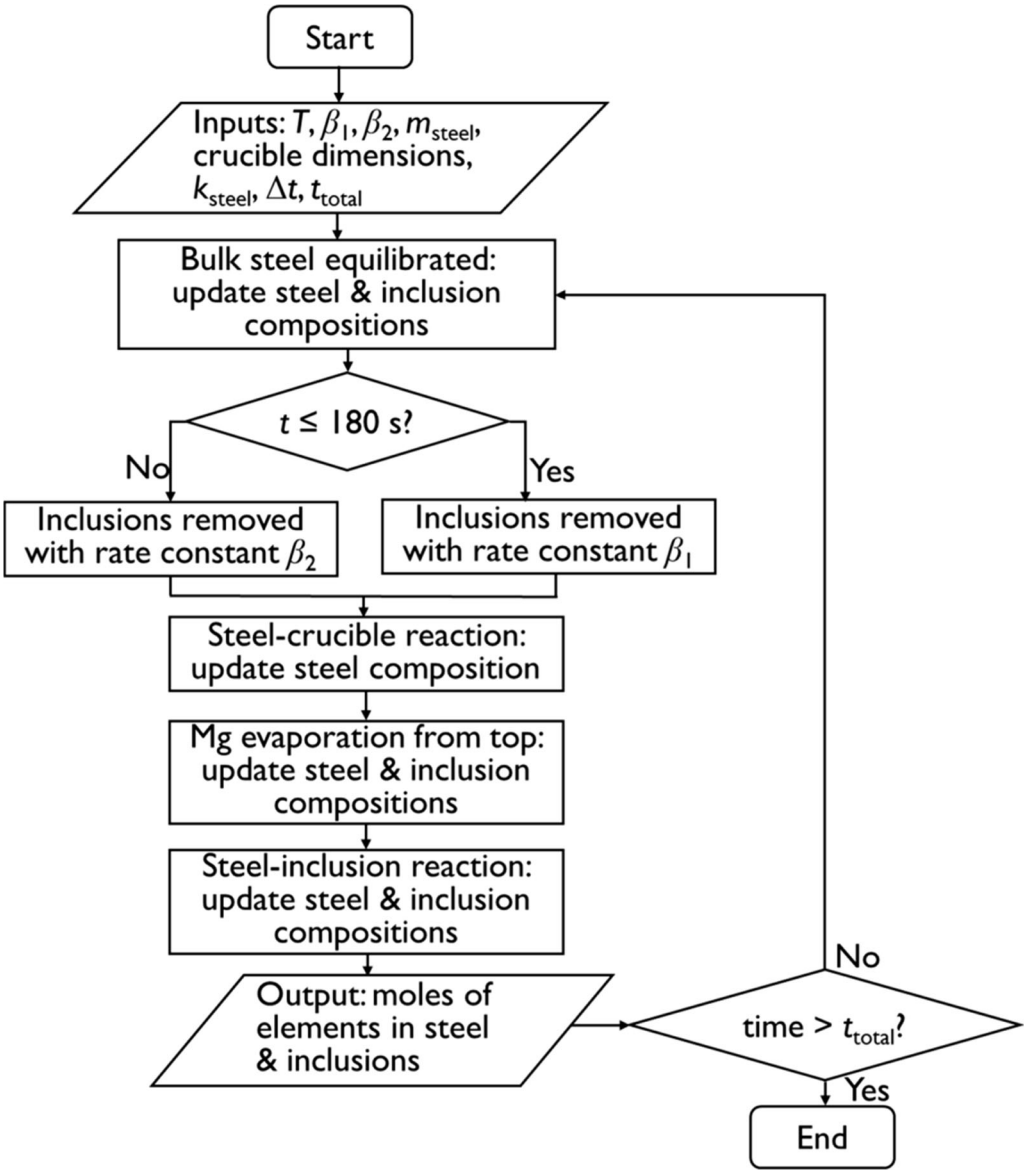

Fig. 3—Schematic of the model calculation procedure.

There were three unknowns in the kinetic model: two inclusion flotation rate constants (β_1 and β_2) and the mass-transfer coefficient in the steel phase for reaction with the crucible. These parameters were estimated from the area and composition of inclusions (measured by automated inclusion analysis).

Figure 3 illustrates the sequence of model calculations. The model was implemented using the macroprocessing feature in FactSage. For the equilibrium calculation, the FTmisc solution database was used for the steel phase (associate model), while the FToxid and Fact-PS (pure substance) databases were used for inclusions.

A. *Inclusion Flotation*

Micron-sized inclusions have very low Stokes velocities; removal of the inclusions relies on stirring in the steel, transporting the inclusions to the slag layer and to the crucible wall. The implication is that inclusion removal is directly related to and dependent on stirring in the liquid steel.[1] In this work, the detail of flow in the liquid steel was not considered directly but was implicitly included in the modeling work as the rate constant of inclusion removal. The overall inclusion removal rate was assumed to follow first-order kinetics (consistent with steel mass-transfer control[1]), as described by Eq. [6]. In this equation, C is the concentration of

inclusions in liquid steel and β is the rate constant. The initial rate of inclusion removal is higher[1] and two rate constants are used, as in previous work[17]: one for large alumina clusters formed just after deoxidation and a second for the remaining inclusions. This is simpler than the approach of Harada *et al.*,[18] who used different flotation rates for alumina, alumina cluster, spinel, and liquid inclusions. The approach used here is similar to that previously used to model inclusion flotation in an industrial ladle, where a single rate constant was fitted to ladle deoxidation (following deoxidation upon tap).[19]

$$\frac{dC}{dt} = -\beta C \qquad [6]$$

B. *Steel-Crucible Reaction*

The rate of reaction between the steel and crucible was considered to be controlled by the mass transfer in steel. To model the mass-transfer-controlled reaction, a fixed fraction of steel was taken to reach the steel-crucible interface in each time-step, to equilibrate with the crucible (Eq. [7]). The effect of crucible impurities was considered in the model by equilibrating the liquid steel with MgO-saturated slag (52 pct CaO, 35 pct Al_2O_3, and 13 pct MgO; 20-μm thick) for crucible type 1 (based on the CaO/Al_2O_3 ratio of 1.5 measured by EDS) and with MgO-saturated spinel for crucible type 2.

$$f_{\text{steel}} = \frac{k_{\text{steel}}\rho_{\text{steel}}A_{\text{crucible}}\Delta t}{W_{\text{steel}}} \qquad [7]$$

In Eq. [7], f_{steel} is the fraction of steel reacting with the crucible in each time-step Δt, k_{steel} is the mass-transfer coefficient in steel, ρ_{steel} is the steel density, A_{crucible} is the steel-crucible contact area, and W_{steel} is the total steel mass.

No calcium-containing inclusions were observed in either of the experiments. Previous studies have shown that the FTmisc database of FactSage tends to overpredict calcium concentration in steel.[17] To avoid this discrepancy, the calcium transfer from slag layer to steel was ignored by deleting Ca and Ca*O (Ca-O associate) end members from the Fe-Liq phase in the FTmisc database.

C. *Magnesium Evaporation*

As magnesium can have a relatively high vapor pressure over the liquid steel melt, some magnesium evaporation may occur. There are two possible interfaces for this under the conditions of these experiments: the top of steel melt (there was no slag) and diffusion of magnesium vapor through pores in the MgO crucible. Evaporation from the top surface was evaluated using an approach similar to that used by Hino *et al.*[20] to quantify the evaporation rate of zinc from liquid iron, considering three steps: magnesium transport from the bulk of liquid steel to the steel-argon interface, evaporation of magnesium at the steel-argon interface, and transport of magnesium in the gas phase. Given the high magnesium vapor pressure (0.025 atm for Fe-0.26 pct Al-7.7 ppm O and $a_{\text{MgO}} = 1$), the Langmuir evaporation rate at the steel-argon interface was not rate determining. The mass-transfer coefficient in bulk steel was fitted to the measured MgO concentration in inclusions for

Table III. Fitted Model Parameters

	Experiment 1	Experiment 2	
β_1	0.007 s^{-1}	0.0091 s^{-1}	inclusion flotation—first step (with reoxidation in experiment 1)
β_2	0.0009 s^{-1}	0.0013 s^{-1}	inclusion flotation—second step
k	5.5×10^{-5}	3.2×10^{-6}	apparent steel mass-transfer coefficient for steel-crucible reaction

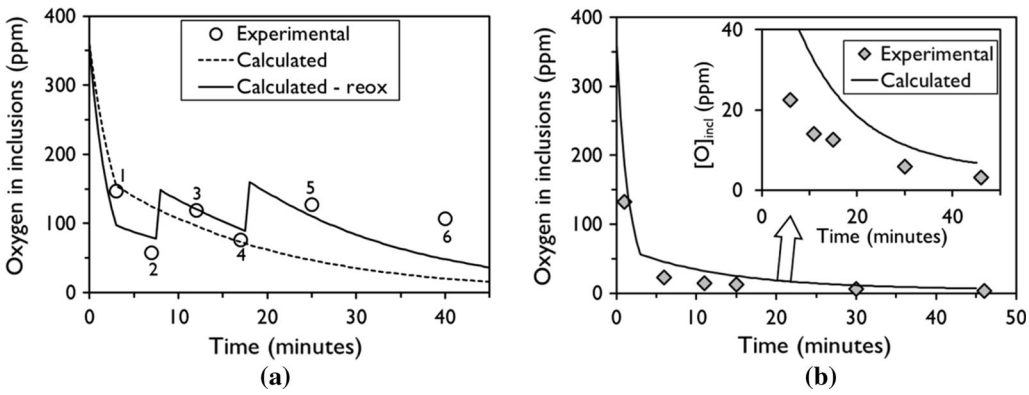

Fig. 4—Measured and fitted amount of oxygen bound in inclusions. (*a*) For experiment 1, assuming 75 ppm of oxygen added by reoxidation (at 8 and 18 min) improves the fit (solid line); numbers 1 through 6 identify sampling times. (*b*) Experiment 2; inset shows fitting of the second flotation rate constant (β_2).

experiment 1 and was equal to 5.5×10^{-5}m/s, as shown in Table III. The gas-phase mass-transfer coefficient was estimated using Eq. [8] for natural convection from a horizontal disk.[21] The binary diffusivity for magnesium vapor in argon at 1873 K was calculated as 5.8×10^{-4}m^2/s, using the method of Poling *et al.*[22] The resulting estimated gas-phase mass-transfer coefficient was equal to 0.12 m/s, much higher than the mass-transfer coefficient in liquid steel, with a slightly smaller concentration difference: $\Delta C_{\text{gas phase}} = 0.16$ mole/m^3 at 1873 K for $p_{\text{Mg}} = 0.025$ atm and $\Delta C_{\text{liquid steel}} = 2.9$ mol/m^3 for $[\text{Mg}]_{\text{dissolved}} = 10$ ppm and a steel density of 7000 kg/m^3. Therefore, mass transfer in the liquid steel was considered to be the rate-controlling step for magnesium evaporation from liquid steel.

Assuming mass transfer in steel to be rate limiting, the magnesium loss rate (in mass ppm/s) was calculated using Eq. [9].

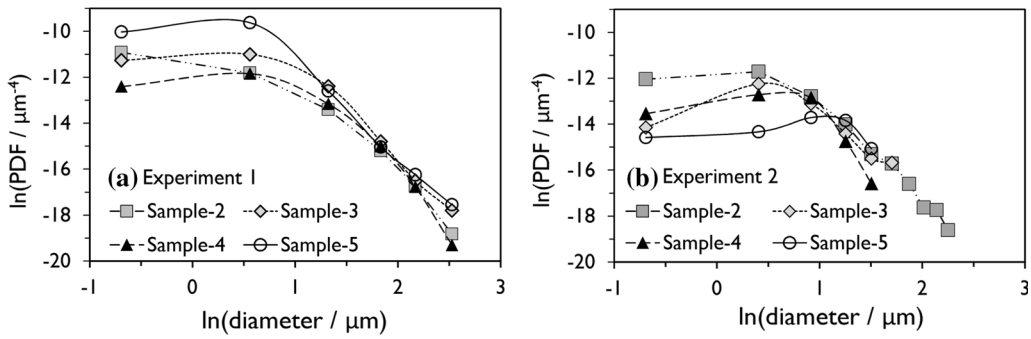

Fig. 5—PDF of inclusions for samples 2 through 5 from (*a*) experiment 1 and (*b*) experiment 2. In (a) experiment 1, the higher concentration of small inclusions in samples 3 and 5 indicates reoxidation.

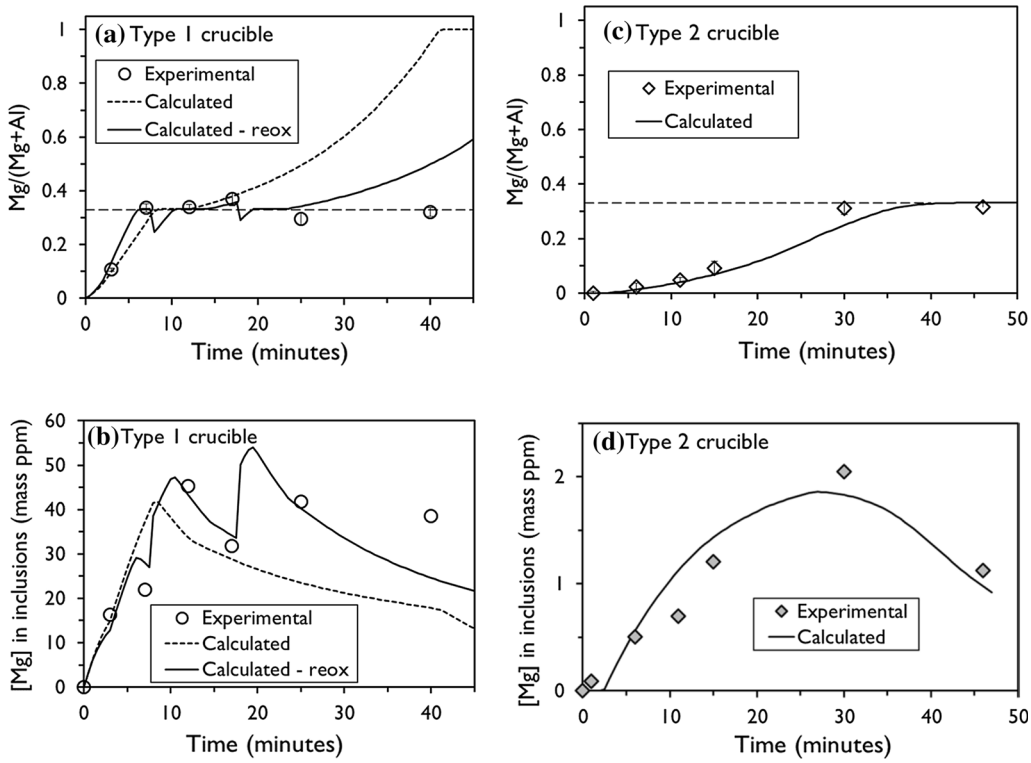

Fig. 6—Measured and modeled changes in Mg concentrations in inclusions, for Al-killed steel in contact with two different types of MgO crucible. Type 1 crucible: (*a*) Mg mole fraction in inclusions and (*b*) total bound Mg in steel. Type 2 crucible: (*c*) Mg mole fraction in inclusions and (*d*) total bound Mg in steel.

$$\mathrm{Sh} = 0.54\mathrm{Ra}^{\frac{1}{4}} \quad [8]$$

where Sh is the Sherwood number and Ra is the Rayleigh number

$$\dot{\mathrm{M}}\mathrm{g}_{\mathrm{loss}} = \frac{k_{\mathrm{steel}} A_{\mathrm{top}} \rho_{\mathrm{steel}} C_{\mathrm{Mg}}}{W_{\mathrm{steel}}} \quad [9]$$

where A_{top} is the projected steel-gas interfacial area and C_{Mg} is the concentration (in parts per million) of Mg in the steel.

An upper bound on the rate of magnesium loss through the porous crucible wall was calculated using an estimated effective pore diffusivity of magnesium vapor. The effective diffusivity was calculated from Mg-Ar binary diffusivity, Knudsen diffusivity (pore size = 5 μm, based on SEM observations), and the porosity of the crucible wall, taking tortuosity to be the reciprocal of the porosity (Eq. [10]). This gives $D_{\mathrm{eff}} = 3.1 \times 10^{-8}$ m^2/s for a crucible porosity of 1 pct, as reported by the supplier and assuming all pores to be open. The magnesium loss rate was estimated using Fick's first law of diffusion for crucible wall thickness = 2 mm (Eq. [11]), giving a rate of approximately 10^{-6} ppm/s for [Mg] = 10 ppm. The conclusion is that magnesium evaporation through the crucible wall was insignificant.

$$D_{\mathrm{eff}} = (\mathrm{porosity})^2 D_{\mathrm{binary}} \quad [10]$$

where

$$D_{\mathrm{binary}} = \frac{D_{\mathrm{Ar-Mg}} \times D_{\mathrm{Knudsen}}}{D_{\mathrm{Ar-Mg}} + D_{\mathrm{Knudsen}}} \qquad J = -D_{\mathrm{eff}}\left(\frac{\Delta C}{\Delta x}\right) \quad [11]$$

D. *Steel-Inclusion Reaction*

As described in previous work, the steel-inclusion reaction is not expected to be limiting under these experimental conditions due to the relatively large steel-inclusion interfacial area and rapid mass transfer around inclusions.[9] In this approach, the steel-inclusion reactions were considered to reach equilibrium in each time-step of the calculation. This approach significantly simplifies the complexity of modeling steel-inclusion reactions since the size distribution of inclusions does not affect the reaction rate. The quantitative basis of the assumption that steel inclusion reactions are close to equilibrium is as follows: The time constant for reaction of steel with a population of inclusions is given by the volume of steel divided by the product mA, where m is the average mass-transfer coefficient to inclusions and A is the total area of all inclusions in the steel.[9] The mass-transfer coefficient for small, approximately spherical inclusions is approximately D/r, where D is the diffusivity in the liquid steel and r the inclusion radius.[9] The total area of all inclusions is given by $4\pi r^2(n_{\mathrm{incl}}/V_{\mathrm{steel}})$, where $n_{\mathrm{incl}}/V_{\mathrm{steel}}$ is the number of inclusions per unit volume of steel. This is given by $n_{\mathrm{incl}}/V_{\mathrm{steel}} = 3(V_{\mathrm{incl}}/V_{\mathrm{steel}})/(4\pi r^3)$, where $V_{\mathrm{incl}}/V_{\mathrm{steel}}$ is the volume fraction of inclusions in the steel. These relationships give the time constant for the steel-inclusion reactions as $r^2/(3DV_{\mathrm{incl}}/V_{\mathrm{steel}})$. Typical values of $r = 1$ μm, $D = 5 \times 10^{-9}$ m^2/s, and $V_{\mathrm{incl}}/V_{\mathrm{steel}} = 10^{-4}$ yield a time constant of 0.7 seconds, which is much smaller than the typical time constant for steel-crucible reactions (several minutes, as shown later) and also smaller than the time-step of 30 seconds used in the simulations.

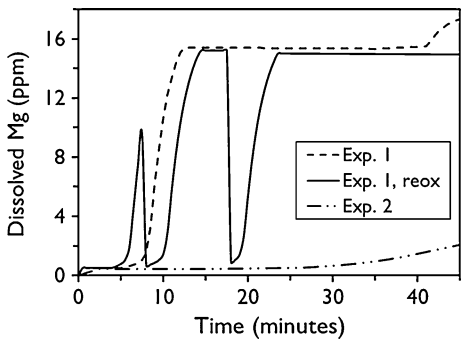

Fig. 7—Calculated change in concentration of dissolved Mg in steel, for a slag-coated MgO crucible (experiment 1, with and without reoxidation) and a spinel-coated MgO crucible (experiment 2).

IV. RESULTS AND DISCUSSION

A. *Inclusion Concentration*

The bound oxygen in inclusions was used to fit inclusion removal rate constants β_1 and β_2 with the fitted lines shown in Figure 4 (Table III for the fitted values). Based on the inclusion removal behavior over many similar experiments,[23] the transition time from β_1 to β_2 was set at $t = 3$ minutes. Inclusion removal could be fitted in this way for experiment 2; the inset in Figure 4(b) illustrates fitting of β_2. However, the fit was not good for experiment 1. A likely reason is that reoxidation had occurred during sampling and affected samples 3 and 5 (Figure 4 for the sample numbers). Reoxidation can occur by inadvertent introduction of air into the furnace chamber when taking the sample. If oxygen contacts the steel, new alumina (and possibly spinel) inclusions would form, increasing the concentration of bound oxygen and forming new, smaller inclusions. Van Ende *et al.*[24] showed that the inclusions generated from reoxidation are expected to have a log-normal size distribution as their sizes are controlled by nucleation and growth; in contrast, sizes are expected to follow a power-law distribution if inclusions change size only by collision and breaking. The population density function (PDF) was calculated for samples 2 through 5 from experiment 1 using Eq. [12].[24]

$$PDF = \frac{n_v(L_{XY})}{L_Y - L_X} \quad [12]$$

where $n_v(L_{XY})$ is the volume density of inclusions (number/m^3) in a particular size range, with $(L_Y - L_X)$ being the width of the size interval. The volume

density of inclusions was calculated from the area density of inclusions (n_A) using $n_v = n_A/\overline{D}$, where $\overline{D}$ is the average diameter of inclusions in that size range.

The calculated PDF for samples 2 through 5 from experiment 1 (Figure 5(a)) shows a larger number density of inclusions for samples 3 and 5 (compared with samples 2 and 4), supporting the idea that reoxidation had occurred before samples 3 and 5 were taken. As indicated in Figure 4, reoxidation was included in the model calculations by assuming addition of 75 ppm of oxygen at both $t = 8$ and 18 min. It should be noted that there was no increase in bound oxygen in inclusions during experiment 2, indicating that there was no significant reoxidation during sampling in that experiment. The absence of reoxidation is supported by the observation that the number of small inclusions did not increase in experiment 2 (Figure 5(b)).

Table IV. Model Parameters for Simulation of Industrial Ladle Processing

Steel Mass	250 tons
Slag Mass	2000 kg
Temperature	1873 K
Steel Mass-Transfer Coefficient	0.002 m/s
Slag Mass-Transfer Coefficient	0.0002 m/s
Steel Density	7000 kg/m^3
Slag Density	3000 kg/m^3
Steel-Slag Projected Interface Area	12.5 m^2
Steel-Refractory Interface Area	43.6 m^2

Table V. Industrial-Scale Simulation Cases Considered: Two Different Inclusion Concentrations, with and without Steel-Refractory Reaction (Steel-Slag Reactions Considered in All Cases)

		Total Oxygen Concentration	
		50 ppm	10 ppm
Steel-Refractory Reaction	yes	case 1	case 3
	no	case 2	case 4

B. *Magnesium Transfer to Inclusions*

Figure 6 gives the measured and modeled changes in inclusion composition—expressed as the Mg/(Mg + Al) molar ratio—and the total [Mg] bound in inclusions. (As noted earlier, the inclusion compositions and amounts were obtained by automated inclusion analysis.) Alumina inclusions transformed to spinel inclusions during both experiments but at a much higher rate with the slag-coated (type 1) crucible. Including the effect of reoxidation (model results shown as solid lines for the type 1 crucible) improved the agreement between measurements and model results.

The model predicted that the inclusion composition would change beyond spinel to form MgO for the slag-coated crucible. While this change is not evident in the average inclusion composition (likely, in part, because of reoxidation), a few pure MgO inclusions were observed together with spinels. Formation of MgO inclusions in similar Al-containing steels in contact with MgO-saturated calcium aluminate slag has been reported.[25] Transformation of spinel inclusions to MgO is possible because the activity of alumina in the slag ($a_{Al_2O_3} = 0.006$ for the calcium aluminate slag coating considered in this work) is smaller than in MgO-saturated spinel ($a_{Al_2O_3} = 0.06$; activities relative to pure corundum calculated with FactSage), providing a driving force for continued reaction of Al with MgO in the spinel inclusions.

The total magnesium bound in inclusions initially increased (as the alumina inclusions picked up magnesium) and later decreased (because of removal of inclusions by flotation and evaporation of magnesium). The contribution of evaporation to magnesium removal was much smaller (less of the total 10 pct) than inclusion flotation. The change in the concentration of bound magnesium was used to fit the mass-transfer coefficient in steel for the steel-crucible reaction; the fitted mass-transfer coefficients are given in Table III. The lower apparent steel mass-transfer coefficient for reaction with the spinel-coated crucible (experiment 2) indicates that diffusion of MgO through the spinel layer was also rate limiting. The presence of the spinel coating would also have an equilibrium effect: Because the

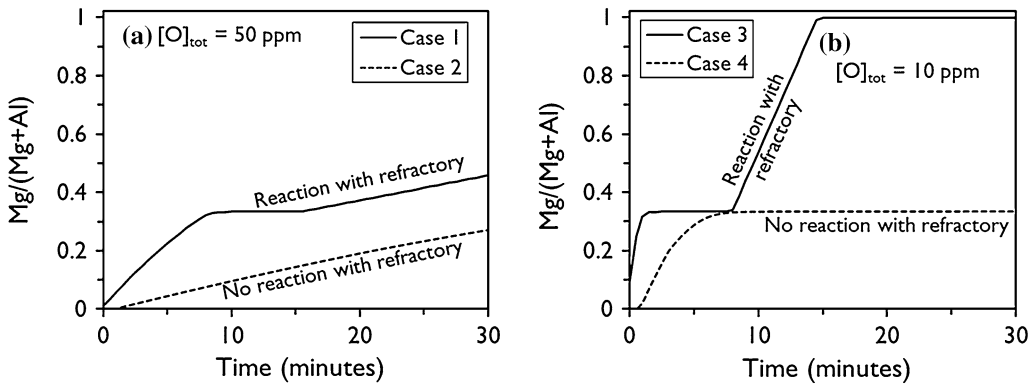

Fig. 8—Predicted MgO pickup by inclusions in Al-killed steel during ladle processing for steel containing (*a*) 50 ppm total oxygen and (*b*) 10 ppm total oxygen, if the steel reacts with both slag and refractory (solid lines—cases 1 and 3) or slag only (broken lines—cases 2 and 4).

Al_2O_3 activity in the spinel layer is approximately 10 times that in the slag coating (and considering the reaction stoichiometry given in Eq. [2]), the Mg concentration in the steel at the steel-crucible interface would be approximately $10^{1/3} \approx 2$ times lower for a type 2 (spinel-coated) crucible. The difference in reaction rate (for type 1 and type 2 crucibles) was much larger than this; the spinel layer also had a significant retarding effect on the inherent kinetics of Mg pickup by the steel.

As shown in Figure 7, the calculated concentration of dissolved magnesium at earlier times was expected to be very low, indicating magnesium evaporation was not significant at those times. Therefore, a constant and steep increase in magnesium content in inclusions was observed for early times. However, at later times, significant magnesium loss is predicted to occur by flotation of MgO containing inclusions (and, to a minor extent, by magnesium evaporation).

C. *Practical Implications*

The kinetic model that was developed to simulate steel-refractory-(slag)-inclusion reactions under laboratory conditions was used to explore some industrial-scale implications of magnesium pickup. In one set of calculations, the expected contributions of steel-refractory reactions and the diluting effect of a higher inclusion concentration were assessed. In another set, the inevitability of spinel formation during ladle desulfurization was tested.

D. *Relative Contributions of Slag and Refractory*

Assumed model parameters are listed in Table IV. The mass-transfer coefficient in steel was the same for steel-slag and steel-refractory reactions, and the mass-transfer coefficient in the slag was 10 times smaller than these.[9] The mass-transfer coefficient in steel was 0.002 m/s, based on previous work.[19] In the plant, the steel-refractory reaction can be expected to vary depending on the choice and quality of refractories and the presence and composition of ladle glaze (which would reflect slag chemistry control in each individual plant). Typically, ladle slag contains CaO, Al_2O_3, MgO, and SiO_2 and traces of FeO and MnO but would vary depending on plant and steel grade needs. As noted by Liu *et al.*,[5] the MgO-C refractory may contain Al_2O_3-SiO_2-CaO impurities. In the current set of simulations, the refractory was assumed to be coated by a ladle glaze with the same composition as the laboratory experiments (52 pct CaO, 35 pct Al_2O_3, and 13 pct MgO), as an example. This would be realistic for refractory coated by ladle slag from a previous heat. The liquid steel was Al killed with 0.05 pct total Al and a total oxygen concentration of 50 or 10 ppm. The slag composition was 51.2 pct CaO, 41.6 pct Al_2O_3, and 7.2 pct MgO, close to double saturation with CaO (a_{CaO} = 0.96) and MgO (a_{MgO} = 0.99).[10] Four conditions were simulated (Table V) to illustrate the diluting effect of total oxygen concentration (and, hence, the initial alumina inclusion concentration) and the relative contribution of refractory and slag to inclusion transformation. Inclusion flotation was not considered in order to observe the effect of total oxygen more readily. The only other difference from the simulations of the laboratory-scale reactions was the addition of steel-slag reaction (in addition to reaction of steel with slag-coated refractory).

Figure 8 shows the calculated increase in the Mg^{2+} cation fraction in inclusions during ladle processing. (An increase in Mg/(Mg + Al) from 0 to 0.33 is the transformation from alumina to stoichiometric spinel inclusions, and from 0.33 to 1, spinel transforms to MgO.) The transformation rate is predicted to be approximately 4.5 times higher if the steel-refractory reaction is considered (case 1) than for only the steel-slag reaction (case 2), which is the ratio of steel–(slag + refractory) area (56 m^2) to steel-slag area (12.5 m^2). Inclusions transform faster if the total oxygen concentration is lower (Figure 8(b)) because the magnesium flux from the steel– (slag + refractory) reactions is absorbed by a smaller relative mass of oxides.

From this analysis, slag-coated refractory can be a significant source of magnesium. The use of alumina refractory in contact with steel is expected to help in avoiding spinel formation; the role of ladle glaze remains to be confirmed for industrial conditions.

The simulations predict an arrest once inclusion composition reaches stoichiometric spinel (Mg/[Mg + Al] = 0.33). Figure 9 illustrates that the arrest results from an increase in the concentration of dissolved Mg in equilibrium with the inclusions, caused by changes in the activity of Al_2O_3 (decreasing) and MgO (increasing) in the oxide inclusions. The dissolved magnesium concentration remains very low during transformation of alumina to spinel when the Al_2O_3 activity in inclusions remains high (and MgO activity is low). The FactSage database predicts that corundum would be present (together with Al_2O_3-saturated spinel solid solution) up to Mg/(Mg + Al) = 0.2; for inclusions transformed beyond this ratio, the concentration of dissolved Mg increases (Figure 9). Modifying the inclusions beyond stoichiometric spinel requires a higher concentration of dissolved magnesium; as Figure 9 shows, the arrest (in the change in inclusion composition) occurs while the [Mg]

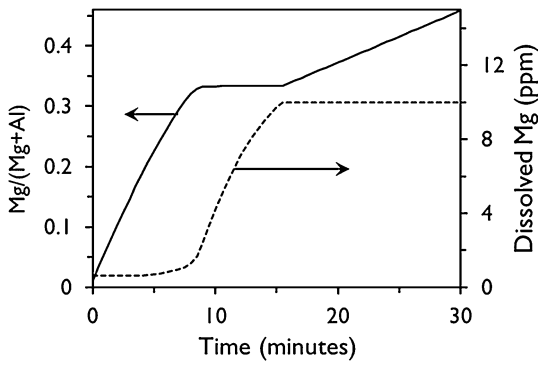

Fig. 9—Calculated change in inclusion composition and dissolved magnesium with time for case 1.

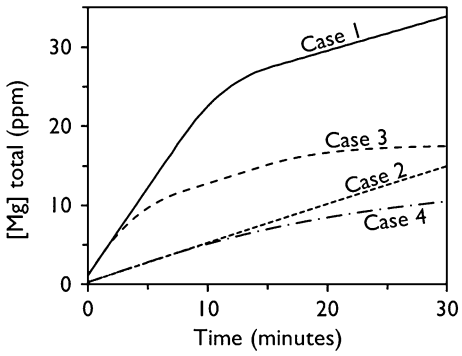

Fig. 10—Calculated increases in total Mg (dissolved and in inclusions) for the four industrial simulation cases of Table V.

increases—supplied by the steel—(slag + refractory) reactions—to that defined by the MgO-$MgAl_2O_4$-[Al] equilibrium.

In all cases, substantial increases in total magnesium are predicted (Figure 10); the total magnesium pickup would depend on the reacting area (steel-slag only, or steel-refractory too) and the availability of inclusions to absorb magnesium. The extent of pickup would affect inclusion formation during possible reoxidation after calcium treatment: As noted by Verma *et al.*,[26] the calcium modification of spinel inclusions causes reduction of MgO from spinel inclusions, resulting in an increase in dissolved magnesium concentration. If such steel containing dissolved magnesium were to undergo reoxidation, spinel inclusions would reappear.[6,26] From the present work, it is noted that if inclusions were not completely transformed to spinel, the dissolved magnesium concentration (and, hence, total magnesium concentration in steel) would be much smaller. Calcium modification of such partially transformed spinel inclusions is expected to result in a much smaller increase in dissolved magnesium concentration, limiting the possibility of spinel formation. This strategy may help in avoiding the reappearance of spinel inclusions during a reoxidation event after calcium treatment.

E. *Desulfurization and MgO Pickup in Inclusions*

Plant data show that MgO pickup by alumina inclusions occurs in parallel with desulfurization of steel; both reactions are favored by a low oxygen potential at the steel-slag interface and by stirring.[27] The current kinetic model was used to test this link for conditions similar to those used by Cicutti *et al.*[27] The initial chemical compositions of steel and slag are given in Tables VI and VII, and the other model parameters are provided in Table VIII. The masses of steel and slag were taken from Cicutti *et al.* The mass-transfer coefficient in the slag phase was taken to be one-tenth that in the steel phase; the mass-transfer coefficients are the same as those listed in Table IV, with the addition of inclusion flotation. The inclusion flotation rate constant was taken from a previous work.[19]

The calculated relationship between MgO pickup by alumina inclusions and the extent of desulfurization (Figure 11) is similar to that reported by Cicutti *et al.*[27]: The extent of MgO pickup increases strongly when the extent of desulfurization is greater than approximately 0.5. The extent of MgO pickup by inclusions is higher at the higher temperature because of the endothermic nature of reduction of Mg from slag by Al (Reaction [3]).

Table VI. Initial Steel Composition (Mass Percentages) for Simulating Spinel Formation During Ladle Desulfurization

C	Mn	Si	P	S	Al	O
0.05	0.5	0.2	0.01	0.02	0.04	0.01

Table VII. Initial Slag Composition (Mass Percentages) for Simulating Spinel Formation During Ladle Desulfurization

CaO	Al_2O_3	SiO_2	MgO	FeO	S
57	27	6	8	1	0.1

Table VIII. Model Parameters to Simulate Desulfurization and MgO Pickup in Inclusions

Steel Mass	180 tons
Slag Mass	3000 kg
Steel Mass-Transfer Coefficient (k_{steel})	0.002 m/s
Slag Mass-Transfer Coefficient (k_{slag})	0.0002 m/s
Inclusion Flotation Rate Constant (β)	0.0026/s
Density of Steel	7000 kg/m^3
Density of Slag	2500 kg/m^3

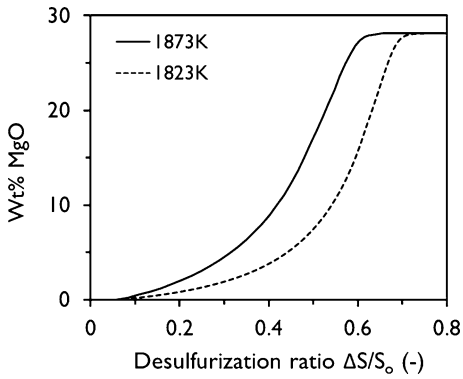

Fig. 11—Calculated relationship between MgO pickup in inclusions and the extent of desulfurization during ladle refining of Al-killed steel at 1823 K and 1873y K.

V. CONCLUSIONS

Aluminum deoxidation experiments were conducted in MgO crucibles using an induction furnace setup, to test transfer of magnesium to alumina (deoxidation) inclusions. A kinetic model was developed, including steel-refractory reaction, steel-inclusion reaction, flotation of inclusions, and magnesium evaporation from the steel surface. Comparison of model calculations with laboratory-scale experimental results provided insight into the rate of transformation of alumina inclusions. The kinetic model was also used to simulate typical steelmaking conditions to illustrate some of possible practical implications. The main conclusions are as follows.

1. Impurities in the crucible can form a liquid slag layer on the crucible wall. The slag layer greatly enhanced magnesium transfer to the steel (and to inclusions in the steel): The transfer rate of magnesium was 20 times higher with a slag layer present, compared with the case when the inner surface of the crucible was coated with a solid (spinel) product layer.
2. The kinetic model can be adapted to reflect the effects of experimental conditions such as reoxidation during the sampling of steel.
3. The bound magnesium in inclusions initially increases due to MgO transfer to inclusions but later decreases due to inclusion flotation.
4. It is expected that under plant conditions, the presence of ladle glaze on MgO-C refractory could significantly accelerate the rate of transformation of alumina inclusions to spinel inclusions, and beyond spinel to MgO. The rate at which inclusions are transformed would be higher if the inclusion concentration were smaller.
5. Under industrial conditions, magnesium pickup by alumina inclusions is expected to be an inevitable side effect of ladle desulfurization of Al-killed steel with a MgO-saturated calcium aluminate slag.

ACKNOWLEDGMENTS

Support of this work by the industrial members of the Center for Iron and Steelmaking Research is gratefully acknowledged. We also acknowledge use of the Materials Characterization Facility, Carnegie Mellon University, supported by Grant No. MCF-677785.

REFERENCES

1. K. Schwerdtfeger: *Arch. Eisenhüttenwes.*, 1983, vol. 54 (3), pp. 87–98.
2. T. Zienert and O. Fabrichnaya: *CALPHAD*, 2013, vol. 40, pp. 1–9.
3. K. Ahlborg: *Steelmaking Conf. Proc.*, ISS-AIME, 2001, pp. 861–69.
4. Z. Deng, M. Zhu, and D. Sichen: *Metall. Mater. Trans. B*, 2016, vol. 47B, pp. 3158–67.
5. C. Liu, F. Huang, J. Suo, and X. Wang: *Metall. Mater. Trans. B*, 2016, vol. 47B, pp. 989–98.
6. J. Tan and B.A. Webler: *AISTech 2016 Proc.*, Association for Iron and Steel Technology, Warrendale, 2016, pp. 2485–96.
7. G. Okuyama, K. Yamaguchi, S. Takeuchi, and K. Sorimachi: *ISIJ Int.*, 2000, vol. 40 (2), pp. 121–28.
8. N. Verma, P.C. Pistorius, R.J. Fruehan, and M. Potter: *Iron Steel Technol.*, 2010, vol. 7 (1), pp. 189–97.
9. S.P.T. Piva, D. Kumar, and P.C. Pistorius: *Metall. Mater. Trans. B*, 2017, vol. 48B, pp. 37–45.
10. C.W. Bale, E. Bélisle, P. Chartrand, S.A. Decterov, G. Eriksson, A.E. Gheribi, K. Hack, I.-H. Jung, Y.-B. Kang, J. Melançon, A.D. Pelton, S. Petersen, C. Robelin, J. Sangster, P. Spencer, and M.-A. Van Ende: *CALPHAD*, 2016, vol. 54, pp. 35–53.
11. A. Harada, G. Miyano, N. Maruoka, H. Shibata, and S. Kitamura: *ISIJ Int.*, 2014, vol. 54, pp. 2230–38.
12. D. Roy, P.C. Pistorius, and R.J. Fruehan: *Metall. Mater. Trans. B*, 2013, vol. 44B, pp. 1095–1104.
13. D. Tang, M.E. Ferreira, and P.C. Pistorius: *Microsc. Microanal.*, 2017, vol. 23, pp. 1082–90.
14. C. Merlet: *X-ray Optics and Microanalysis, 1992: Proc. 13th Int. Congr*, 1992, vol. 1993, pp. 123–26.
15. C. Merlet: *Mikrochim. Acta*, 1994, vols. 114–115, pp. 363–76.
16. *CRC Handbook of Chemistry and Physics*, 99th ed., J.R. Rumble, ed., CRC Press, Boca Raton, FL, 2018.
17. D. Kumar and P.C. Pistorius: *AISTech 2016 Proc.*, Association for Iron and Steel Technology, Warrendale, 2016, pp. 1151–59.
18. A. Harada, N. Maruoka, H. Shibata, M. Zeze, N. Asahara, F. Huang, and S. Kitamura: *ISIJ Int.*, 2014, vol. 54, pp. 2569–77.
19. D. Kumar, K.C. Ahlborg, and P.C. Pistorius: *AISTech 2016 Proc.*, Association for Iron and Steel Technology, Warrendale, 2016, pp. 1151–59.
20. M. Hino, S. Wang, T. Nagsaka, and S. Ban-ya: *ISIJ Int.*, 1994, vol. 34, pp. 491–97.
21. J.R. Lloyd and W.R. Moran: *J. Heat Transfer*, 1974, vol. 96, pp. 443–47.
22. B.E. Poling, J.M. Prausnitz, and J.P. O'Connell: *Properties of Gases and Liquids*, 5th ed., McGraw-Hill, New York, 2001.
23. D. Kumar: Ph.D. Thesis, Carnegie Mellon University, Pittsburgh, PA, 2018.
24. M.-A. Van Ende, M. Guo, E. Zinngrebe, B. Blanpain, and I.-H. Jung: *ISIJ Int.*, 2013, vol. 53, pp. 1974–82.
25. H. Mu, T. Zhang, R.J. Fruehan, and B.A. Webler: *Metall. Mater. Trans. B*, 2018, vol. 49B, pp. 1665–74.
26. N. Verma, P.C. Pistorius, R.J. Fruehan, M.S. Potter, H.G. Oltmann, and E.B. Pretorius: *Metall. Mater. Trans. B*, 2012, vol. 43B, pp. 830–40.
27. C. Cicutti, C. Capurro, and C. Cerrutti: *9th Int. Conf. Exhib. on Clean Steel, Simulation and Model Calculations*, Hungarian Mining and Metallurgical Society (OMBKE), Budapest, 2015.